Ultrafast Dynamics in Microemulsions: Optical Kerr Effect Study of the Dispersed Oil Phase in a Carbon Disulfide−Dodecyltrimethylammonium Bromide−Water Microemulsion

Neil T. Hunt, Andrew A. Jaye, and Stephen R. Meech*

School of Chemical Sciences and Pharmacy, University of East Anglia, Norwich NR4 7TJ, U.K.

Received: October 24, 2002; In Final Form: January 15, 2003

The ultrafast, optically-heterodyne-detected optical Kerr effect has been used to investigate the dynamics of the dispersed oil phase of a novel oil-in-water microemulsion. The carbon disulfide−dodecyltrimethylammonium bromide−water (CS_2−DTAB−H_2O) system has been characterized by viscosity and conductivity measurements. The results of these measurements are discussed in terms of possible shape changes and interparticle interactions. Ultrafast measurements are reported for several different compositions of the microemulsion. The results are compared and contrasted with the dynamics of neat CS_2 and CS_2 dissolved in *n*-alkanes. The dynamics of CS_2 dispersed in the microemulsion do not approach those of the neat liquid in any case, even at the highest possible loading, implying that the dynamics in the oil phase are strongly perturbed by the surfactant. The slow (picosecond) diffusive reorientation of the CS_2 does not reflect the macroscopic viscosity of the microemulsion.

Introduction

Microemulsions are thermodynamically stable, single-phase liquid mixtures.[1] For oil-in-water microemulsions, the oil component is dispersed in the continuous water component as droplets with nanometer-sized dimensions, which are stabilized by interaction with the surfactant. Microemulsions have been intensively studied for more than 30 years, because of both fundamental interest in the behavior of such complex fluids[2,3] and their great practical value, in areas ranging from oil recovery to drug delivery.[4] In particular, a great deal of data has been collected concerning the phase behavior, particle shape, and interparticle interactions in these multicomponent mixtures using NMR, light, and neutron scattering methods.[1,2] These measurements have been complemented by many theoretical models and simulations.[5] More recently, the possibility afforded by microemulsions, of confining reactants in nanometer-sized domains, has attracted a great deal of interest for the preparation of nanometer-scale metallic, semiconductor, and polymer particles.[6]

This paper describes a series of measurements of the ultrafast dynamics of an oil-in-water microemulsion, utilizing the ultrafast, optically-heterodyne-detected optical Kerr effect (OHD−OKE).[7−9] Despite the above-noted widespread interest in microemulsions, there are rather few studies of the dynamics of the dispersed liquid phase. The absence of such data is unfortunate, because it has long been established in studies of solution phase chemistry that an understanding of liquid dynamics is essential to understanding the dynamics of chemical reactions and solvation in the condensed phase.[10−13] Thus, it is expected that a knowledge of the dynamics of the dispersed liquid component will be important in understanding, modeling, and controlling the kinetics of processes such as nanoparticle formation and drug solubilization in microemulsions. The few studies that have addressed the dynamics of the dispersed liquid component of microemulsions, through light scattering, far-IR absorption spectroscopy, or ultrafast fluorescence, are mainly concerned with water-in-oil microemulsions, although a few nonaqueous systems have been studied.[14−20] These results show that the dispersion of water in nanometer-sized micelles can have a dramatic effect on its dynamics, a result that is reproduced by theoretical calculations and molecular dynamics simulations.[21]

The OHD−OKE technique employed here was developed in its most commonly used form by McMorrow, Lotshaw, and their co-workers.[22−32] It has been very widely used to study the ultrafast dynamics of pure liquids and liquid mixtures.[33−61] The method and its applications have been reviewed.[7−9] The key features of the OHD−OKE method are the very high time resolution available from reliable deconvolution procedures and the very high quality data, which arise from the amplification and linearization of the signal resulting from optical-heterodyning. More recently, the method has been applied to record the dynamics of some complex fluids and heterogeneous media, including polymer solutions[62] and liquid crystals.[63] Of most direct relevance to the present work, Fourkas and co-workers recently described a series of measurements of the ultrafast dynamics of liquids confined in nanoporous glasses.[64−68] The effect of pore size and surface hydrogen bonds were investigated for both wetting and nonwetting liquids. Applications of the OHD−OKE method designed to probe a particular component of a heterogeneous sample rely, for their contrast, on the fact that the induced polarizability anisotropy, the relaxation of which is monitored in ultrafast OHD−OKE experiments, scales with the polarizability of the medium.[7−9] Thus, for a porous silicate glass loaded with a highly polarizable liquid (for example, carbon disulfide (CS_2)), the liquid fraction of the sample will dominate the signal.

To benefit from the selectivity of the OHD−OKE method, it is clearly necessary to choose a microemulsion with a dispersed oil phase consisting of molecules of high polarizability. For this reason, we chose to produce a carbon disulfide−dodecyltrimethylammonium bromide−water (CS_2−DTAB−H_2O) microemulsion for this first study of the ultrafast dynamics

* To whom correspondence should be addressed. Author can be reached via E-mail (s.meech@uea.ac.uk).

10.1021/jp022301w CCC: $25.00
Published on Web 03/21/2003

of microemulsions. It has been found (see below) that this system has a phase diagram similar to those of several other oil−DTAB−H_2O microemulsions.[69,70] Although signal strength and contrast were clearly strong motivating factors in the choice of CS_2 as the oil phase, this choice does confer some other advantages. First, CS_2 has been well studied by ultrafast OHD−OKE spectroscopy in the pure liquid phase,[7,27,60] and it has also been studied on dilution in nonpolar alkane solvents.[30−32,54,55,59] These data provide important starting points for the analysis of the microemulsion data. Second, the understanding of ultrafast dynamics in liquids, and their role in controlling the dynamics of chemical reactions, has been greatly aided by comparison with the results of molecular dynamics simulations.[71−73] The CS_2 molecule has been the subject of several such investigations,[74−77] and it may be that its choice as the oil phase will facilitate molecular dynamics simulations of the microemulsion (although the alkyl chains of the surfactant will no doubt present a considerable challenge). Third, this new microemulsion might have some interesting properties in terms of solubilizing solutes; CS_2 is not dipolar but has a high quadrupole moment and, therefore, exhibits strong intermolecular interactions. Finally, it should be noted that, although we are not aware of any other detailed investigations of the CS_2−DTAB−H_2O system, we cannot claim absolute precedence: a single report (from less environmentally conscious times) of the application of a CS_2−oleic acid−ethanol−cottonseed oil−basic water mixture as a suitable pesticide for control of the Japanese beetle (*Popillia japonica*) has been published.[78]

The remainder of this paper is structured as follows. In the Experimental Section, the standard OHD−OKE setup is described, with the modifications made to it to allow the collection of reliable data from samples yielding relatively small signals. The methods employed in the preparation and characterization of the microemulsions are also outlined. In the third section, the macroscopic properties of the microemulsion are discussed, followed by presentation of the OHD−OKE data, their analysis, and discussion in terms of the dynamics of neat and dilute CS_2. The paper ends with some conclusions and description of future directions.

Experimental Section

The basic OHD−OKE spectrometer employed in this work has been described in detail elsewhere.[41] As a result of the rather low concentrations of CS_2 present in the microemulsion samples studied, it was necessary to make several changes to enhance both the dynamic range and the signal-to-noise ratio (S/N). Such improvements became particularly important in light of the observed multiexponential dynamics of the long-time relaxation of the microemulsions (see below).

The experimental arrangement is shown schematically in Figure 1 and is based upon that developed by Fourkas and coworkers to study the dynamics of bulk liquids constrained in nanoporous glasses.[64−68] The light source was a Kerr lens modelocked titanium sapphire laser (Clark-MXR) operating at 800 nm with a repetition rate of 100 MHz, pumped by the 532 nm, 4.25 W output of a $NdYVO_4$ laser. This produced, with the aid of a dispersive delay line to compensate for group velocity dispersion, nearly transform limited pulses ∼45 fs in duration, as measured by second-order autocorrelation at the sample position.

The laser beam was first passed through a half-wave plate, to achieve vertical polarization, before being incident on a beam splitter, yielding two separate beams in the intensity ratio of 95:5, labeled the pump and probe beams, respectively. The latter

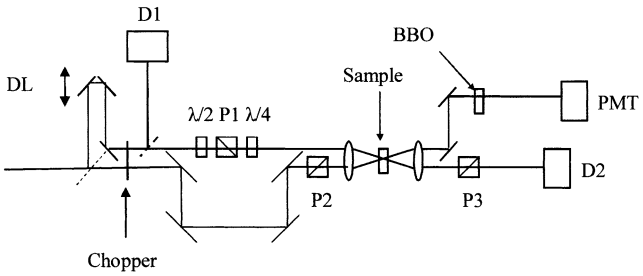

Figure 1. Schematic diagram of the experimental arrangement. Legend is as follows: D1 and D2, reference and signal diodes of balanced photoreceiver, respectively; DL, delay line; $\lambda/2$ and $\lambda/4$, half and quarter wave plates; P, polarizer; and PMT, detector for the reference second harmonic signal.

was routed through a variable delay line before the two beams were passed through the inner and outer rings of a two-ring chopper. With the outer ring operating at 1.4 kHz, this enabled the OHD−OKE signal to be demodulated at the difference of these two frequencies, ∼250 Hz. Demodulation at the difference frequency served to remove the constant background signal due to scattered pump beam radiation.

After the chopper, an additional beam splitter (90:10) was placed in the probe beam path. The weaker reference beam was directed onto the silicon reference diode of a balanced photoreceiver unit (New Focus, model 2007). The remainder of the probe beam and the pump beam were then arranged in the standard OHD−OKE geometry[7−9] with the probe polarization oriented at 45° to the pump beam. In addition, the angle of the first polarizer in the probe beam (P1) was rotated by an additional 1.5°, creating the out-of-phase local oscillator necessary for heterodyne detection. The samples were housed in quartz cuvettes with a path length of 1 mm.

After the sample, the probe and associated signal beams were directed onto the signal diode of the balanced photoreceiver and the reference signal was subtracted. Although the balanced photoreceiver features automatic balancing electronics, as opposed to a simple subtraction, the effect is to recover the full dynamic range of the lock-in amplifier, as reported earlier by Loughnane et al.[64]

To normalize the signal against low-frequency laser intensity fluctuation, the transmitted pump beam was picked off and focused into a frequency-doubling crystal. The resulting 400 nm radiation, which shared the quadratic dependence upon laser intensity of the OHD−OKE signal, was detected using a photomultiplier tube and lock-in amplifier. The signal from the balanced detector was then divided by this reference signal. This normalization proved extremely useful for reliable detection of the small signals found at particularly large delay times, up to 20 ps, for these CS_2-containing samples. The entire measurement and collection apparatus was under computer control via LabView software.

Short-time-scale data were recorded using a resolution of 1.3 fs per step, taking the average of five scans. For the longer-time data, lower time resolution could be used (33−133 fs per step); however, as a result of the weaker signals, more averages were required. Typical spectral acquisitions were on the order of five averages per stage position per scan and up to 20 scans.

Analytical-quality CS_2 (Fisher), DTAB (Lancaster, 97% purity), heptane (Aldrich, 99.9%), and dodecane (Lancaster, 99.9%) were used without further purification. The water used to form the microemulsions was purified via a Millipore filtration system. All samples were passed through 0.2 μm filters prior to use, to remove any dust particles, and were allowed to equilibrate at the laboratory temperature, 295 ± 1 K.

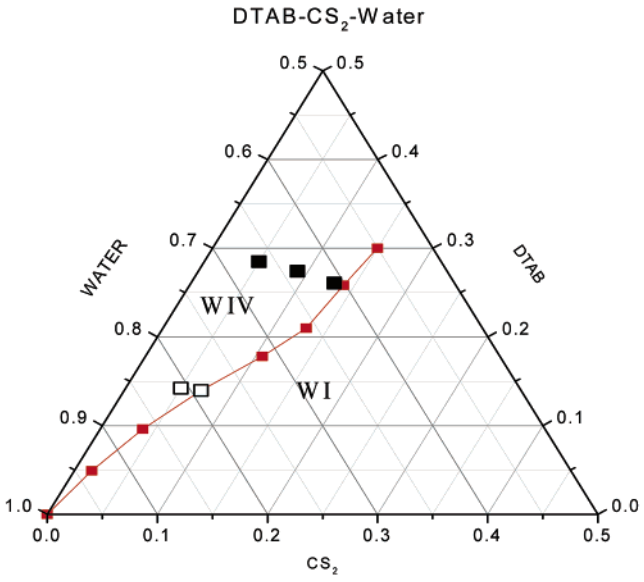

Figure 2. Portion of the CS_2−DTAB−H_2O phase diagram showing the boundary of the monophasic microemulsion regime (WIV, see text) and the samples studied. Open squares represent 15 wt % DTAB, and solid squares represent 30 wt % DTAB samples. Red squares correspond to points on the phase boundary obtained experimentally.

The microemulsions studied here were formed by the addition of CS_2 to a solution of DTAB dissolved in water. Gentle stirring for a few minutes produced an opaque mixture that cleared rapidly to yield an optically pure single-phase microemulsion at any composition up to the phase boundary. Figure 2 shows the relevant portion of the phase diagram for the CS_2−DTAB−H_2O system and indicates the composition of the samples studied by OHD−OKE. It should be noted that the relevant phases are labeled in accordance with established practice: namely, the monophasic microemulsion region is called Winsor IV (WIV) and the biphasic region consisting of oil over an oil-in-water microemulsion is labeled Winsor I (WI). The position of the phase boundary was determined via titration of CS_2 into a range of DTAB−H_2O solutions at 298 K. Upon reaching the boundary, the above-mentioned initial turbidity persisted indefinitely. Figure 2 also shows the points on the phase boundary determined in this manner.

Two series of microemulsions were studied using OHD−OKE spectroscopy, and these are referenced in terms of the initial amount of DTAB dissolved in water prior to addition of CS_2, namely 15 and 30 wt %. In each case, an attempt was made to obtain microemulsions containing a range of CS_2 concentrations. In practice, the number of samples was restricted by the need for observable signals at the lower boundary and by the onset of the biphasic region of the phase diagram at the upper. The microemulsions studied were 5 and 7 wt % CS_2 in 15 wt % DTAB (denoted 5/15 and 7/15, respectively) and 5, 9, and 13 wt % CS_2 in 30 wt % DTAB (5/30, 9/30, and 13/30, respectively). For completeness, the compositions of these microemulsions are described in Table 1, in terms of the volume fraction of the dispersed phase and of the mole fractions.

Although too concentrated to be studied using simple dynamic light-scattering experiments, these microemulsions were characterized using conductivity and viscosity measurements. All measurements were performed at 295 K on samples that had been allowed to equilibrate over a period of 24 h. Viscosity measurements were carried out using two Ubbelohde-type viscometers of different capillary size, to ensure maximum accuracy. In each case, the quantity measured was the relative viscosity, η_{rel}, where

$$\eta_{rel} = \frac{\eta_{solution}}{\eta_{solvent}} = \frac{t_{solution}}{t_{solvent}} \quad (1)$$

and t_x corresponds to the flow time of component x through the viscometer's capillary.

TABLE 1: Characterization Data for the Microemulsions Studied, Including Volume Fraction of the Dispersed Phase (ϕ), Mole Fractions (x), and Micelle Occupation Numbers (N)

microemulsion label	ϕ_{CS_2}	x_{CS_2}	x_{DTAB}	$N_{CS_2}{}^a$ (micelle^{-1})
5/30	0.038	0.017	0.024	30
9/30	0.069	0.032	0.024	66
13/30	0.101	0.047	0.023	100
5/15	0.039	0.014	0.010	61
7/15	0.055	0.020	0.010	101

[a] Based on a DTAB aggregation number of 50 (see text).

Results and Discussion

(1) Viscometry and Conductivity of the CS_2−DTAB−H_2O Microemulsion. The viscometry data (Figure 3) are presented as a plot of reduced viscosity, η_{red}, versus the volume fraction of dispersed phase, ϕ. The reduced viscosity is defined as

$$\eta_{red} = \frac{1}{\phi}\left(\frac{\eta_{solution}}{\eta_{solvent}} - 1\right) \quad (2)$$

such that the plot of η_{red} versus ϕ will be linear, according to the Einstein equation:[79]

$$\frac{\eta_{solution}}{\eta_{solvent}} - 1 = K\phi + k_1\phi^2 + ... \quad (3)$$

An intercept of 2.5 as $\phi \rightarrow 0$ is indicative of a near-spherical particle shape.[79] Positive deviations from a linear plot are expected at higher volume fractions of spherical particles, because of higher-order contributions to eq 3 and interparticle interactions, or at any ϕ for nonspherical particles. It should be noted prior to further discussion of the results that the dispersed phase includes both the surfactant and any tertiary component (in this case, CS_2) and, as a result, each value of ϕ is unique to a given system. For this reason, the microemulsions discussed below generally are defined in terms of the weight percentage of CS_2, as described in section 2. The value of ϕ can easily be calculated, if desired, from the data given in conjunction with the densities of CS_2 (1.26 g cm^{-3}, from ref 87) and DTAB (0.87 g cm^{-3}). The latter value is actually that for the chloride (dodecyltrimethylammonium chloride, DTAC) rather than the bromide (DTAB) but was used in the absence of an accurate value for DTAB.

Figure 3a shows the conductivity and viscometry data for binary mixtures of DTAB and water. It can be seen that the conductivity increases monotonically as DTAB is added to the water. This is as expected, upon increasing the ionic character of the solution. In contrast, the viscometry data show a significant positive deviation from the linearity expected on the basis of eq 3. This is especially marked at $\phi > 0.35$. Previous studies of DTAB micelles in brine using small angle neutron scattering (SANS)[80] and fluorescence decay of DTAC micelles in water[81] suggested a spheroidal shape with a major:minor axis ratio in the region of 1.3:1. This is then one possible source of

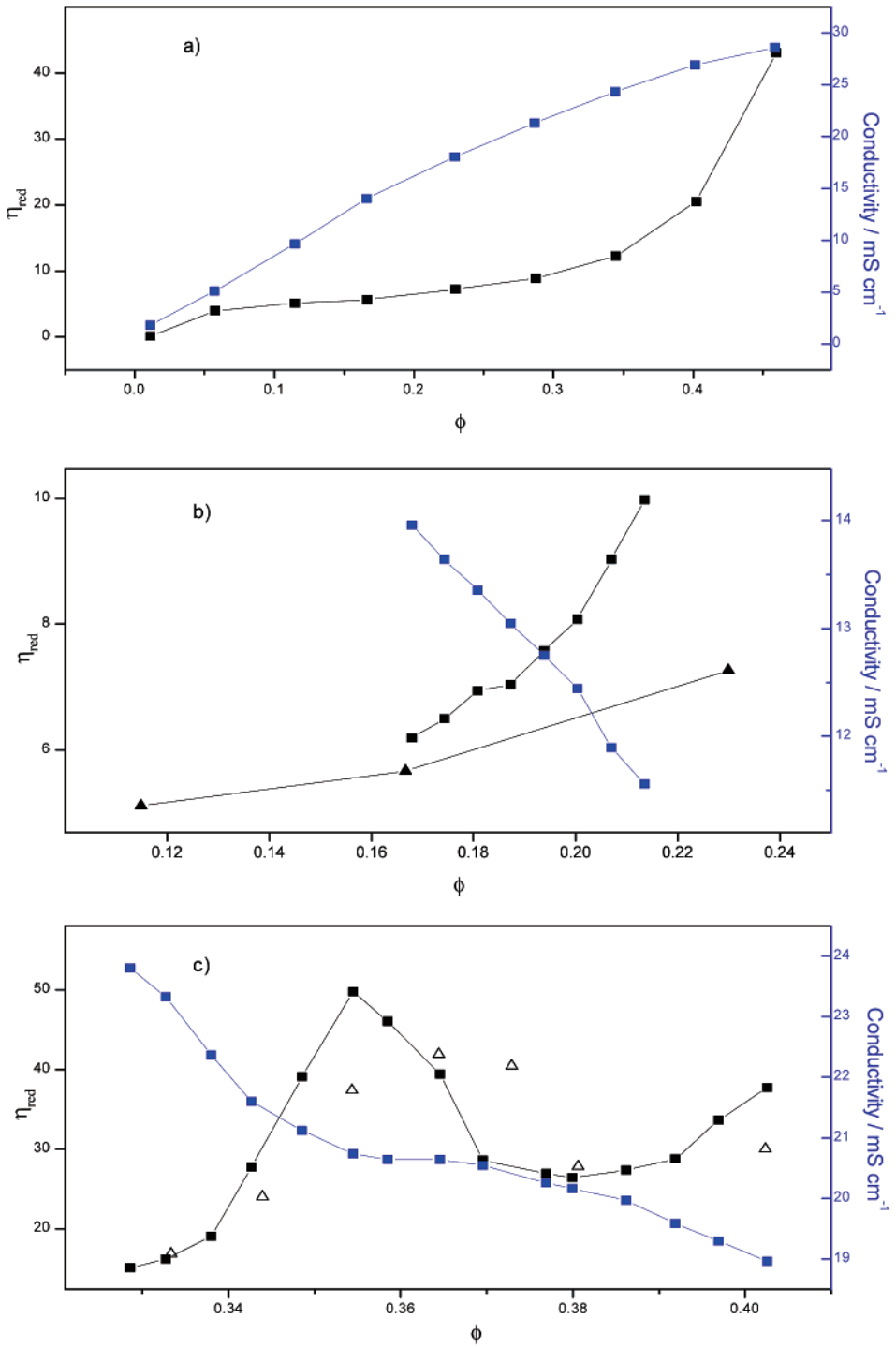

Figure 3. Conductivity (blue data) and viscometry (black data) results for (a) DTAB/H_2O (ϕ range corresponds to 1−40 wt % DTAB), (b) 15 wt % DTAB microemulsions (ϕ range corresponds to 0−7 wt % CS_2), and (c) 30 wt % DTAB microemulsion family (ϕ range corresponds to 0−14 wt % CS_2). Closed triangles in panel b represent DTAB/H_2O binary mixture viscosity data for comparison. Open triangles in panel c represent viscosity data taken with a second viscometer with a narrower capillary.

nonlinearity. It has also been reported[79] that higher-order terms in the Einstein equation can be significant at high values of ϕ, which may also explain the deviations observed.

It is however interesting to note that, at ϕ values of 0.05−0.35, the viscometry data are quite linear and, indeed, on extrapolation, intercept the axis close to a value of 2.5. It would therefore seem reasonable to conclude that the DTAB micelles are almost spherical, even at high values of ϕ. It is noteworthy that the 15 wt % DTAB microemulsion lies comfortably within the linear portion of the viscosity curve, whereas the 30 wt % example lies near the upper bounds of the linear regime (a value of 15 wt % corresponds to a ϕ value of 0.17, and a value of 30 wt % corresponds to $\phi = 0.35$).

The addition of CS_2 to a mixture of 15 wt % DTAB in water leads to a more marked increase in viscosity, in comparison to simple DTAB micelles, accompanied by a decrease in conductivity (Figure 3b). The deviation of the viscometry data from the predictions of eq 3 can be attributed to higher-order contributions to eq 3 at large values of ϕ, and possibly stronger interactions between the larger micelles, a factor not accounted for in eq 3. Although the data are nonlinear, the increase in viscosity is monotonic and therefore unlikely to herald any

change in micelle morphology on CS_2 addition. The decrease in conductivity is an expected consequence of the increased viscosity of the medium, leading to a change in diffusion rates.

The conductivity and viscometry measurements for the microemulsions based on 30 wt % DTAB solutions (Figure 3c) reveal somewhat different, and more complex, trends, compared to 15 wt % DTAB solutions. Again, the conductivity is reduced with the addition of CS_2, but a plateau is observed at $\phi \approx 0.36$. This result is reflected in the viscometry data, which show a sharp rise to a peak near $\phi = 0.35$, followed by a decrease in viscosity, as ϕ increases further, and a subsequent steady increase up to the maximum values of ϕ studied. One possible explanation lies in a change in microemulsion morphology upon reaching a certain fraction of the dispersed phase: for example, a change from spheroidal to spherical could lead to the anomalous decrease in viscosity with increasing ϕ.

A similar anomalous maximum in viscosity was observed by Bergenholtz et al.[82] for the water-in-oil microemulsion Aerosol OT−H_2O−*n*-decane system. A combination of viscometry and SANS was used, which allowed the effect to be attributed to disorder at the surfactant/water interface[82] rather than to changes in particle morphology. In simple terms, the swelling of the surfactant micelle on addition of the tertiary component led initially to the area per surfactant headgroup becoming anomalously large. The greater separation, it was proposed, allowed alkyl chains from neighboring micelles to interlock to a greater extent, increasing interparticle interactions. As more water was added, reordering of the surfactant molecules returned the headgroup areas to normal, thereby reducing the interparticle interactions. Though observed on a different system, the similarities with the data in Figure 3c indicate that an analogous effect may be being observed in the 30 wt % DTAB system.

Also included in Figure 3c are the data on the same samples recorded using a second viscometer with a smaller capillary. These show a similar trend, confirming that the effect is not an artifact of the viscometer. The discrepancies between the two sets of data arise mainly at higher viscosities and are attributable to the smaller diameter of the capillary in the second viscometer; the smaller capillary was less suited to accurate determination of $t_{solution}$ for the more viscous solutions.

The interesting and anomalous phenomenon revealed in Figure 3c is not yet fully understood and would clearly benefit from further study. Neutron or light scattering techniques are good candidates to reveal morphology effects and interparticle interactions, although, as noted earlier, the high micelle concentration makes the analysis of such data nontrivial.

Whatever the cause of this anomalous behavior, it was established that the studied microemulsion solutions remained optically isotropic for all CS_2 concentrations studied, because no depolarization of the laser beams was observed as a function of ϕ. Such depolarization would be expected if the microemulsions crossed a phase boundary into a lamellar region, for example.

An alternative and potentially informative means of characterizing the microemulsion samples is in terms of the number of CS_2 molecules per micelle. This is a nontrivial calculation, because no means of counting micelles is available. It is however possible to apply a very simple model based on the previously reported aggregation number of DTAB in H_2O, which implies that each micelle in the binary mixture contains 50 DTAB molecules.[83] The number of micelles prior to addition of CS_2 can then be calculated. If it is assumed that this number of molecules remains constant upon formation of the microemulsion, then a molecules-per-micelle figure can be obtained. The results of such calculations lead to occupation numbers of 61 and 101 for the 5/15 and 7/15 samples, respectively, along with values of 31, 66, and 100 for the 5/30, 9/30, and 13/30 microemulsions, respectively. Although useful as a discussion tool, such a model does not take into account any changes in the number of DTAB molecules as the micelles become swollen with CS_2 or any changes in shape. As a result, the numbers reported are merely indicative.

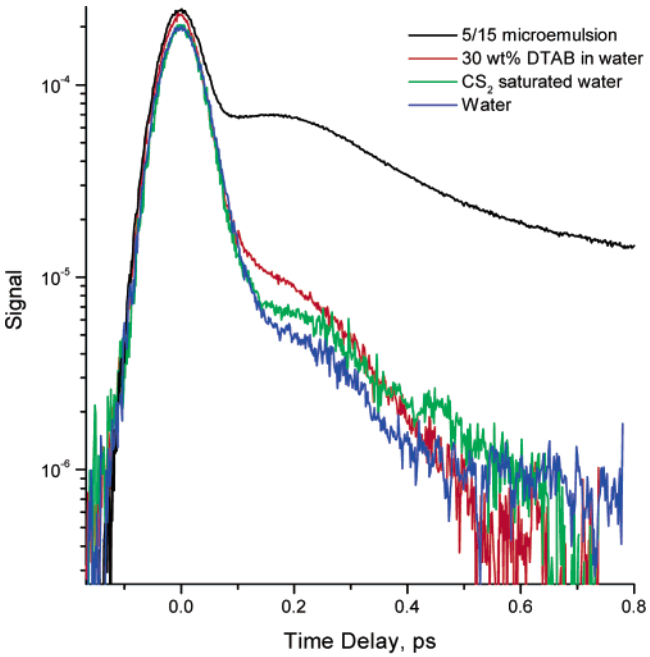

Figure 4. Comparison of subpicosecond OHD−OKE responses of 5/15 microemulsion, 30 wt % DTAB/H_2O binary mixture, CS_2 saturated water, and neat H_2O.

(2) Ultrafast Dynamics. The ultrafast dynamics of CS_2 have been measured in the pure liquid phase, diluted 10 wt % in two *n*-alkane solvents and dispersed in DTAB−H_2O micelles at five different weight fractions, as indicated on Figure 2. Before proceeding with a description of these results, evidence for the selectivity of the OHD−OKE method for CS_2 over other components in the mixtures should be described. In Figure 4, relative intensity measurements of the OHD−OKE signals are shown for pure H_2O, H_2O saturated with (largely immiscible) CS_2, a 30% DTAB−H_2O micelle solution, and a 5/15 microemulsion, the lowest fraction of CS_2 studied here. The data were recorded sequentially under identical conditions. The selectivity of the OHD−OKE method for the dispersed oil component of the microemulsion is clearly demonstrated; CS_2 completely dominates the signal at all times >100 fs. Figure 4 also shows that the signals from other components of the microemulsion drop below the detection limit at rates that are greater than that of the relaxation of the CS_2 component. This result is important when considering the long-time relaxation observed in the microemulsions (see below). Also apparent from Figure 4 is that even the maximum amount of CS_2 dissolved in H_2O contributes a negligible (although nonzero) intensity to the signal at >200 fs. There is also a small but measurable contribution from the DTAB micelles above the signal associated with pure H_2O. The DTAB signal exhibits a shoulder at ca. 200 fs, followed by a subpicosecond relaxation. In all cases, these signals were considered to be too small to necessitate compensation for them in the recorded data.

Some of the time-resolved OHD−OKE data are shown in Figure 5. At approximately time zero, an instantaneous response

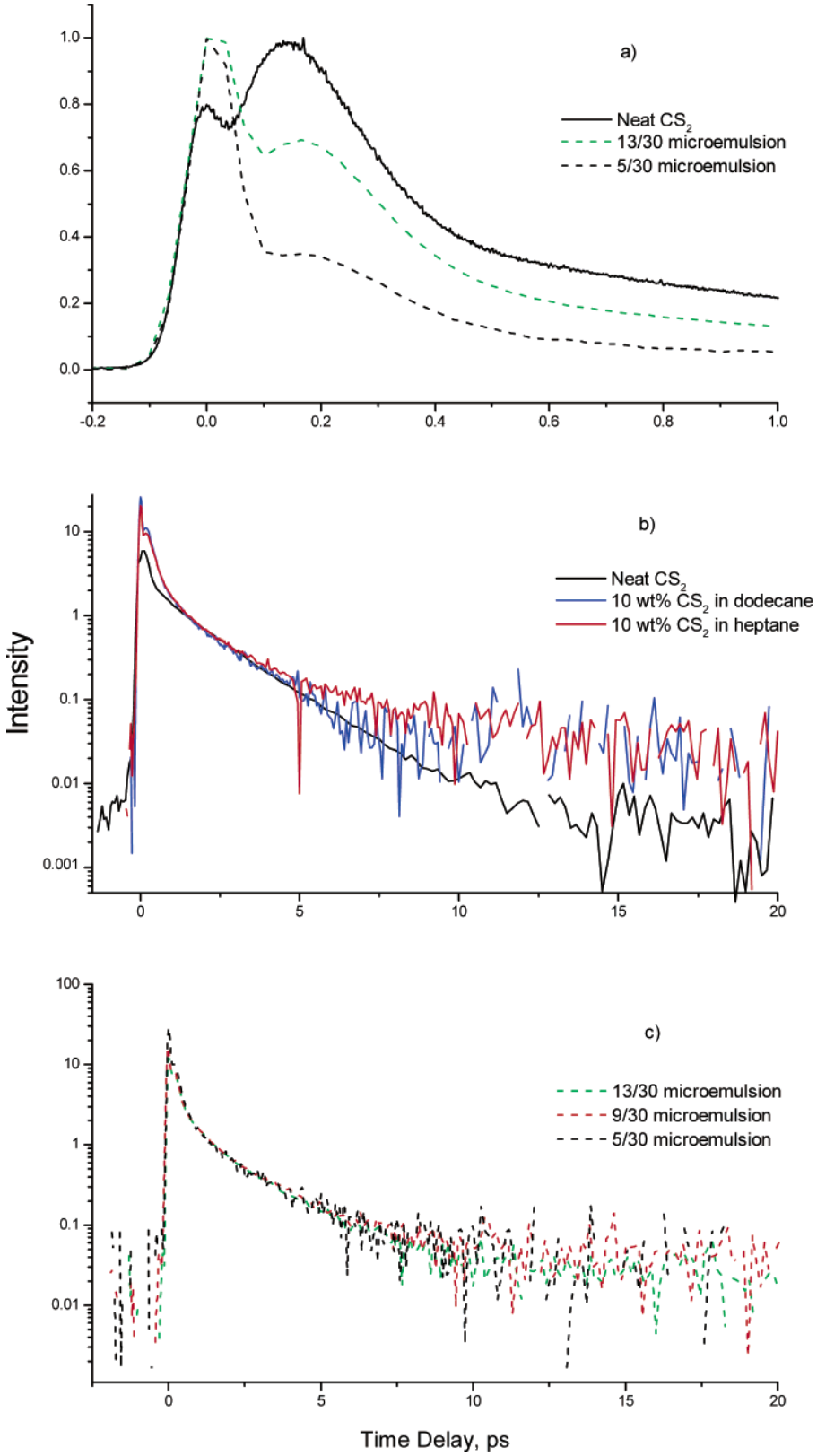

Figure 5. (a) Subpicosecond-time-domain OHD−OKE spectra of neat CS_2, 13/30, and 5/30 microemulsions. (b) Picosecond-time-domain OHD−OKE spectra for neat CS_2 and 10 wt % mixtures. (c) Picosecond-time-domain OHD−OKE spectra of 13/30, 9/30, and 5/30 microemulsions.

is seen in all samples, which has a width that reflects that of the laser autocorrelation and contains contributions from all components in the sample (Figure 4). This is an electronic response and contains no information on the nuclear dynamics of interest here.[7−9] On the remainder of the subpicosecond time scale (Figure 5a), the nuclear (noninstantaneous) response of CS_2 first increases, reaches a maximum, and then decays. The intensity of the nuclear response, relative to the electronic response, decreases as the fraction of CS_2 in the microemulsion decreases, as expected. Also discernible in these data is a shift to later times in the maximum of the nuclear response with decreasing fraction of CS_2 in the sample. A similar shift was

TABLE 2: Results of Long-Time-Scale Exponential Fits to OHD−OKE Spectra According to Eq 5, alongside fwhm and First Moment[a] Values for Nondiffusive Spectral Densities and Sample Viscosities

sample	fwhm (cm^{-1})	$\tilde{\nu}_{av}$ (cm^{-1})	$a_1/(a_1+a_2)$ (%)	τ_1 (ps)	τ_2 (ps)	η ($\times 10^{-3}$ kg m^{-1} s^{-1})
neat CS_2	60.1	43.4	100	1.67		0.32[b]
10 wt % in dodecane	45.0	36.6	94	1.36	11.4	1.02[b,c]
10 wt % in heptane	39.7	32.7	92	1.24	9.2	0.33[b,d]
13/30 microemulsion	50.3	39.1	94	1.36	8.03	11.63
9/30 microemulsion	49.6	38.2	94	1.44	10.4	9.02
5/30 microemulsion	48.8	38.5	80	0.94	3.46	15.11
7/15 microemulsion	51.1	41.4	84	0.86	3.88	2.54
5/15 microemulsion	48.1	39.1	87	0.76	3.30	2.12

[a] See text. [b] From ref 87. [c] Dodecane viscosity measured as 1.25×10^{-3} kg m^{-1} s^{-1}. [d] Heptane viscosity measured as 0.35×10^{-3} kg m^{-1} s^{-1}.

observed on dilution of CS_2 by nonpolar solvents (10% CS_2 in *n*-heptane and dodecane), as was already noted in earlier studies.[30−32,54] The significance of these shifts is most easily discussed on transformation of the ultrafast data to the frequency domain (see below).

When viewed on a longer time scale, the complexity of the relaxation dynamics of both the CS_2/nonpolar solvent and the microemulsions becomes apparent (Figure 5b and c). In all cases, the instantaneous contribution and the rapid rise of the nuclear (CS_2) response are followed by a complex relaxation profile. Even in the case of neat CS_2, it has been established that the relaxation contains at least three components: <200 fs, ca. 500 fs, and 1.6 ps.[31] These are all apparent in the data for neat CS_2 included in Figure 5b, which are in excellent agreement with literature data.[7,27,60] The slowest exponential relaxation time of neat CS_2 has been assigned to diffusive molecular reorientation, on the basis of its linear dependence on η/T.[60] The two faster relaxation times have been variously assigned, as will be discussed further below.

The interesting point from Figure 5b and c is that, upon dilution in nonpolar solvents or dispersal in a microemulsion, the picosecond-time-scale dynamics of CS_2 are no longer well represented by a single-exponential function. For neat CS_2, the slowest component dominates the relaxation for times >2 ps and is rigorously exponential. A 1.67 ± 0.05 ps relaxation time is recovered from a fit to a single-exponential function, independent of the initial time chosen for the fit (provided this is >1.5 ps, to avoid the subpicosecond components). In contrast, the picosecond relaxation dynamics of both solutions and the microemulsions are not single-exponential functions and require at least two exponential components to be accurately fit, with evidence for relaxation times appreciably longer than 1.6 ps. The results of an analysis of the data in terms of two exponentially relaxing components are shown in Table 2.

For both solutions and microemulsions, this analysis recovers a dominant (ca. 90%) relaxation time that is shorter than that of pure CS_2, plus a minor long component. There are previously reported observations of biexponential relaxation for CS_2 dissolved in hexadecane and tetradecane.[30] The two relaxation times reported in hexadecane were 4 and 25 ps.[30] These observations are qualitatively consistent with the present data in dodecane. It was also reported that the slowest relaxation time for CS_2 in *n*-pentane was rigorously exponential.[30] These results led McMorrow et al. to propose that the observed biexponential decay was a characteristic of CS_2 dissolved in long-chain nonpolar solvents, which, it was suggested, arose from a heterogeneous distribution of CS_2 in those solvents. The present data (Figure 5b and Table 2) suggest that the onset for this behavior is the C_7 chain of *n*-heptane. Additional measurements of the picosecond relaxation dynamics of 20% CS_2 solutions in methanol, isopentane, carbon tetrachloride, and dodecane solvents have been made. These data (not shown) confirm that the biexponentiality observed is, indeed, a consequence of alkyl chain length. The picosecond dynamics observed in all solvents other than dodecane, which have properties ranging from nonpolar nonpolarizable through highly polarizable to polar and hydrogen bonding, were well described by a single-exponential relaxation.

It has also previously been reported that the slowest exponential relaxation time for CS_2 dissolved in alkanes reflects its rotational diffusion time,[31,55] and, thus, the relaxation times obey the modified Debye−Stokes−Einstein equation:

$$\tau_c = \frac{g_2 V \eta}{kT} \tag{4}$$

in which τ_c is the collective reorientation time measured by OHD−OKE (and other Raman techniques); g_2 is the static orientational pair correlation parameter, which scales between the collective and single molecule relaxation times (as measured by NMR, for example); and V is the hydrodynamic volume.[84,85] In eq 4, the usual assumption has been made: the dynamical orientational correlation parameter, j_2, may be set equal to one.[84] The conclusion that eq 4 provides a good description of the slowest relaxation time was reached on the basis of studies of neat CS_2 over an extended temperature (and, hence, viscosity) range[60] as well as on the basis of dilution in *n*-alkanes.[31,55] In the latter case, a much narrower viscosity range was available, and the analysis is complicated by the dependence of g_2 on dilution:[59] at infinite dilution, $g_2 = 1$. Although the analysis of the data in Table 2 is further complicated by the nonexponential nature of the relaxation in the long-alkyl-chain solvents, it is not possible to describe the dominant, shorter component recorded here by eq 4. For example, using the data for neat CS_2, and assuming $g_2 = 1.5$, as inferred by Loughnane et al. on the basis of NMR and OHD−OKE data,[61] a hydrodynamic volume of 1.4×10^{-29} m^3 results. This, in turn, predicts relaxation times of 3.5 and 1.14 ps for 10% solutions of CS_2 in dodecane and *n*-heptane, respectively (assuming $g_2 = 1$ for these dilute solutions). These are quite different from the observed dominant relaxation times, yet considerably faster than the minor slow relaxation time (Table 2).

Instead of varying according to eq 4, the data show that, for dilution in both nonpolar solvents, the dominant relaxation time decreases slightly on dilution, compared to neat CS_2, and a second longer relaxation time, with a small weight, appears. It is proposed that these unexpected observations are most easily understood on the basis of an inhomogeneous distribution of environments for CS_2 molecules within long (greater than C_7) chain *n*-alkane solvents, as proposed earlier by McMorrow et al.[30] It is very difficult to be specific about the form and origin of the inhomogeneous distribution, and we are reduced to

speculation. The existence of pools of CS_2 within the long, entangled *n*-alkane chains, which thus encounter a lower effective viscosity than measured macroscopically, is one plausible distribution, which may account for the persistence of a fast relaxation time in viscous media. However, the pools certainly do not have bulklike character (see below). It is furthermore possible, by an extension of the preceding speculation, to assign the slow component to minority CS_2 molecules located at the CS_2−hydrocarbon chain interface of the pool. Such speculations might be amenable to testing by molecular dynamics simulation.

The picosecond relaxation dynamics seen for CS_2 in microemulsions (Figure 5c, Table 2) are qualitatively similar to those observed on dilution in long-chain *n*-alkanes, comprising a dominant fast relaxation that is faster than that of neat CS_2 and a minor additional component several picoseconds in duration. An important point to note here is that the macroscopic viscosities of the microemulsions are higher, often considerably higher, than those of the *n*-alkane solutions (Table 2). The fact that relaxation on the time scale of a few picoseconds persists in all the microemulsions illustrates that bulk viscosity and microscopic relaxation times are largely decoupled in these systems. The macroscopic viscosity reflects interparticle interactions, whereas dynamics in the dispersed oil phase reflect intermolecular interactions at the microscopic level. It is these interactions that will be the most important in understanding chemical reactions in microemulsions and that the current experiments interrogate.

Figure 5c shows that the picosecond dynamics of CS_2 in microemulsions are essentially independent of composition. The data extracted from the biexponential fit suggest some differences, particularly a decrease in the dominant shorter relaxation time when the amount of dispersed CS_2 is small (Table 2). However, as pointed out previously, a constant aggregation number and a statistical distribution of CS_2 molecules are expected to lead to microemulsions of similar composition for the CS_2/DTAB fractions of 7/15 and 13/30. Thus, we believe that the differences seen in Table 2 reflect both the lower S/N value available from the smaller amount of CS_2 (a factor apparent in Figure 5c) and the inadequacy of a biexponential model for the description of the inhomogeneous distribution of CS_2 environments. Attempts have been made to fit the data taken from samples with the highest fractions of CS_2 (9/30 and 13/30) to a sum of three exponential components (again, the fitting starts at 1.5 ps). The quality of the fit is improved, compared to that of the two exponential analyses. In each case, a relaxation time of ca. 500 fs, one of ca. 1.8 ps, and a much longer (>15 ps) component of small amplitude are recovered. However, we regard this analysis as further evidence that the picosecond relaxation is more heterogeneous than can be described by two components, and we attach no significance to the numerical results, other than to suggest that the distribution of relaxation times may span the subpicosecond to 10-ps range in the microemulsion. Further attempts to fit the data to the stretched exponential or Kohlraush function, $r(t) \propto \exp -(t/\tau)^{\beta}$, where $0 < \beta < 1$, were made. This function can be useful in describing a distribution of relaxation times. The best fit to the microemulsion data yielded $\tau = 0.12 \pm 0.2$ ps, with $\beta = 0.4$. However, in no case was the quality of the fit superior to that obtained with two exponentially decaying terms. Hence, subsequent discussion will refer solely to the data reported in Table 2.

The discussion of the ultrafast dynamics (Figure 5a) is most easily conducted by transforming the data into the frequency domain, to yield the Raman spectral density (which are formally identical to the data recorded in Rayleigh wing or dynamic light scattering experiments, apart from a thermal occupation factor[7−9,51]). The analysis procedure was introduced in a series of papers by McMorrow, Lotshaw, and their co-workers[7,23,26] and has since been used by several groups.[33−49] The effects of convolution of the sample response with the finite width of the laser autocorrelation are removed by recording both the OHD−OKE data, $I(t)$, and the second-order autocorrelation, $G^{(2)}(t)$, of the laser pulse (at the sample position). The deconvoluted sample response in the frequency domain, $D(\omega)$, is then obtained from the ratio of the Fourier transforms of these two measurements. To obtain the spectral density for an entire OHD−OKE trace, the long biexponential relaxation time of $I(t)$ is extended, using the fitting parameters obtained from the biexponential analysis.[23,25] To obtain the nondiffusive spectral density, the slow dynamics, assigned to rotational diffusion, are represented by

$$r_{\mathrm{diff}}(t) = [a_1 \exp(-t/\tau_1) + a_2 \exp(-t/\tau_2)][1 - \exp(-2\omega_{\mathrm{av}}t)] \quad (5)$$

in which ω_{av} is the mean frequency of the spectral density. This function is first subtracted from the measured $I(t)$, which are then extended by "zero padding". In either case, the extension of the time domain data improves resolution in the calculated frequency domain spectral densities. The resulting $D(\omega)$ contains both the nuclear dynamics of interest and the instantaneous electronic response. The latter is purely real, so the deconvoluted nuclear dynamics can be isolated by taking the imaginary part of the ratio, $\mathrm{Im}(D(\omega))$. The deconvoluted nuclear response in the time domain, $r(t)$, may then be recovered, if desired, from an inverse complex Fourier transform.

The complete (ultrafast plus diffusive) spectral densities are shown in Figure 6a−c for neat CS_2 and its solutions in *n*-alkanes, the 30% DTAB microemulsion, and the 15% DTAB microemulsion, respectively. The data for neat CS_2 are in excellent agreement with published data, and the origin of the large difference between neat and solvated CS_2 has been discussed before.[30−32,54,55,59] The data for neat CS_2 clearly comprise two components (as was also seen in the time domain, Figure 5b): a sharp peak near zero frequency, which arises mainly from the diffusive response (cf. Figure 7a below), and a broad high-frequency wing, extending beyond 100 cm^{-1}. The latter is associated with the nondiffusive response, e.g., molecular libration and intermolecular interactions. Figure 6a shows that the low-frequency contribution is markedly less well resolved for 10% CS_2 in *n*-heptane and is barely discernible in dodecane. The difficulty in resolving the low-frequency diffusive component for the solutions is associated with two factors. First, the increased inhomogeneity in the diffusive response, mentioned previously, leads to a broadening of the low-frequency peak. At the same time, the ultrafast spectral density shifts to lower frequency (see below and refs 30−32).

In regard to the spectral densities of the microemulsions (Figure 6b,c), these may be considered to be intermediate between those associated with the neat and 10% solutions of CS_2. In particular, the low-frequency edge of $\mathrm{Im}(D(\omega))$ displays a sharp rise, similar to that seen for the neat liquid. However, the low-frequency peak is only very poorly resolved from the broad wing on the high-frequency side, as was found for the solutions. It is also noteworthy that, as the loading of CS_2 increases, the low-frequency component becomes somewhat better resolved, i.e., the microemulsion spectral density approaches that of the neat liquid. *However, the spectral density does not truly resemble that of the bulk liquid at any composition*

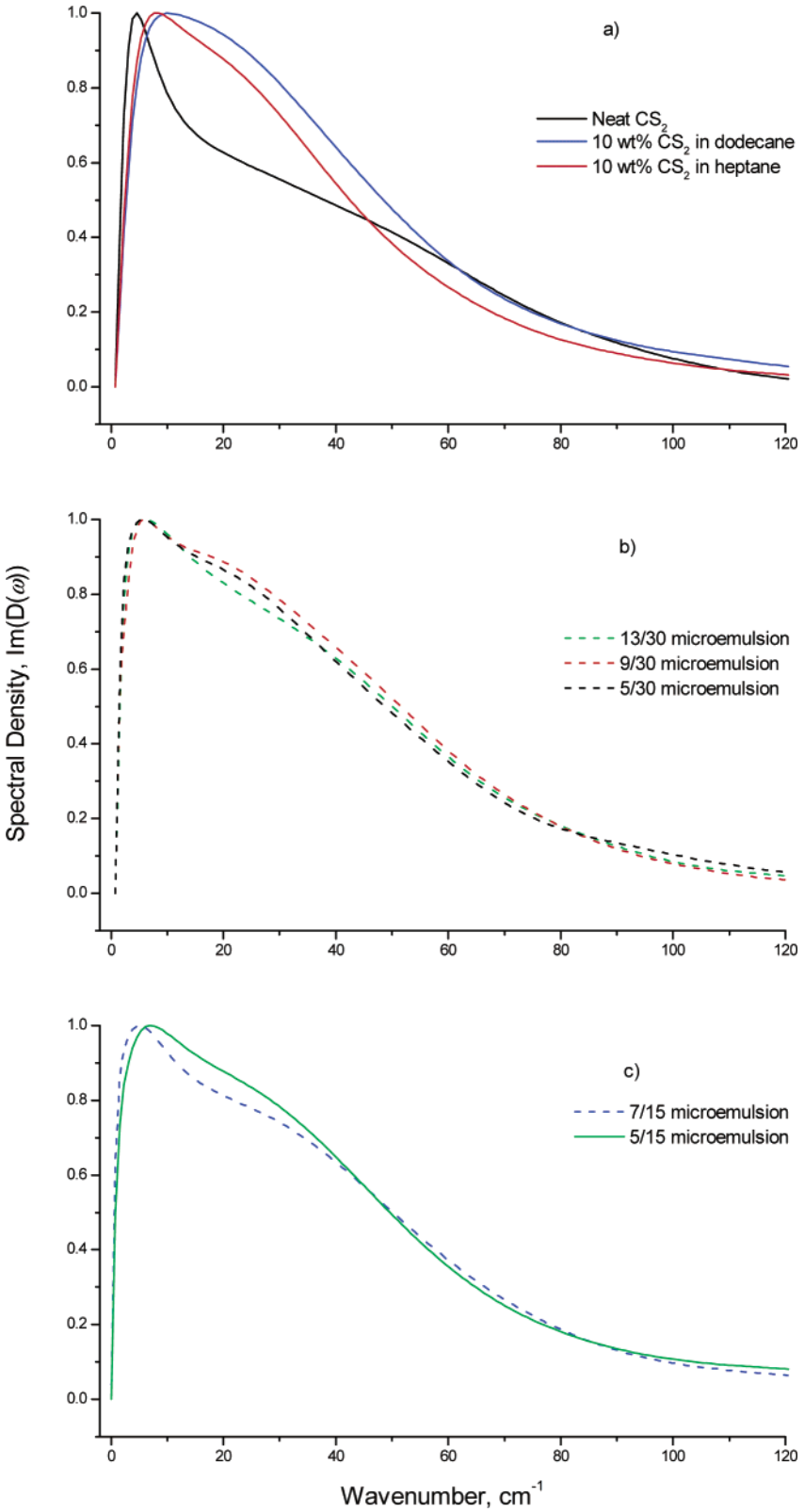

Figure 6. Non-tail-subtracted spectral densities of (a) neat CS_2, 10 wt % CS_2 in dodecane, and 10 wt % CS_2 in heptane; (b) 13/30, 9/30, and 5/30 microemulsions; and (c) 7/15 and 5/15 microemulsions.

of CS_2 in the microemulsion. This is true even for the 13/30 and 7/15 samples, which are at the boundary of phase separation. This leads to the important conclusion that, for the dispersed oil phase of an oil-in-water microemulsion comprising non-dipolar (but highly polarizable and quadrupolar) molecules, such as CS_2, the liquid dynamics are strongly perturbed, compared to the bulk liquid at all compositions; in this case, the oil phase cannot be regarded simply as a microscopic pool of the neat liquid. It is noteworthy that this result contrasts with the observation for liquids confined in nanoporous glasses, where the dominant effect was on the picosecond dynamics.[64−68]

The equivalent nondiffusive spectral densities to Figure 6 have been calculated and are shown in Figure 7. It should be noted that, generally, the justification for the separation of the diffusive

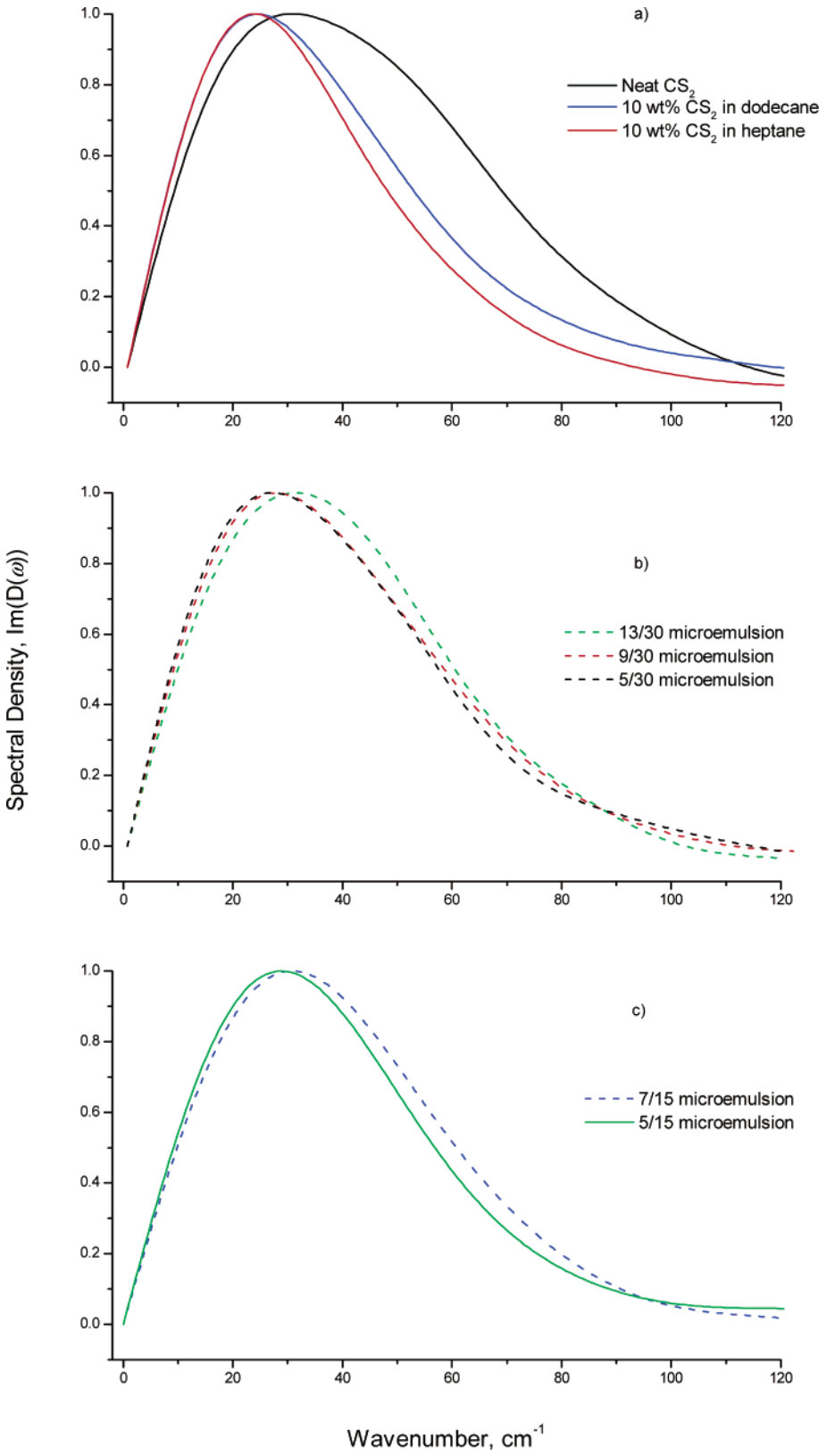

Figure 7. Tail-subtracted spectral densities of (a) neat CS_2, 10 wt % CS_2 in dodecane and 10 wt % CS_2 in heptane; (b) 13/30, 9/30, and 5/30 microemulsions; and (c) 7/15 and 5/15 microemulsions.

and nondiffusive dynamics is the large separation in time scales between them. Even in neat CS_2, the separation is not extremely large but is justified by the rigorously exponential long-time decay, which is well fit by eq 4. When the diffusive dynamics are described by a distribution of relaxation times, as is the case for the samples studied here, this separation becomes increasingly difficult to justify. To minimize the possibility of introducing a systematic error, we subtract a diffusive response (eq 5) from all the data sets using the parameters derived from a biexponential analysis (Table 2), rather than the three component analyses, even though these gave better fits in some cases. The ultrafast Im($D(\omega)$) functions so derived are character-

ized in Table 2 by their width and mean frequency.

$$\tilde{\nu}_{av} = \int_0^\infty \tilde{\nu} D(\tilde{\nu})\, d\tilde{\nu} / \int_0^\infty D(\tilde{\nu})\, d\tilde{\nu}$$

Qualitatively, some trends are apparent from Figure 7. As already noted by two groups, the dilution of CS_2 in alkanes leads to a shift of Im($D(\omega)$) to lower frequency, accompanied by a significant decrease in halfwidth. These changes have been reported to be gradual and become saturated when the volume fraction of CS_2 reaches 20%, a value below which no further significant shifts are seen.[30,54] Our data are again in excellent agreement with the literature. All the spectral densities for the microemulsions show behavior intermediate between that of neat CS_2 and its 10% solutions. For example, the mean spectral width is 49 cm^{-1} for the microemulsions, compared to 60 and 45 cm^{-1} for neat CS_2 and CS_2 diluted in dodecane, respectively. The variations within a series of microemulsion loadings are much smaller. However, the small broadening and shift to higher frequency of Im($D(\omega)$) (Figure 7b,c) as the composition approaches the phase boundary were reproducible for both 15% and 30% DTAB solutions. This is again consistent with the dynamics of the dispersed CS_2 phase approaching (but never reaching) that of the neat liquid. It is also interesting to note that a large change of composition (e.g., between 13% and 5%) yields only small changes in Im($D(\omega)$). This is contrary to the behavior in solutions, where width and mean frequency are very sensitive functions of the fraction of CS_2 (at least down to 20%[54]). One explanation for this observation is that the local density of CS_2 in the microemulsion remains more or less unchanged by composition and, with increasing amounts of CS_2, the pools simply increase in size.

Further analysis of the frequency of the microemulsion spectral densities, and their changes in shape as a function of composition, can be made in terms of existing analyses of the behavior of CS_2 on dilution.[54,32] This is somewhat complicated, because the origin of the ultrafast spectral density, even in neat CS_2, is not definitively assigned and has been the subject of much debate. It is established that there are numerous possible contributions to the signal. For example, even a first-order approximation, which considers permanent and dipole−induced dipole contributions to the collective polarizability, yields six terms.[55] Furthermore, these contributions depend differently on dilution. However, this complex picture notwithstanding, there is wide agreement that the major component of the nondiffusive response arises from a single intermolecular vibrational (librational) mode, such that, to a first approximation,

$$r(t) = r_{libr}(t) + c \cdot r_{diff}(t) \qquad (6)$$

where $r(t)$ represents the third-order response function (for the nuclear dynamics) and c is a constant.[54,32]

Duppen and co-workers developed an expression for $r_{libr}(t)$ based on a quantum mechanical harmonic oscillator representation of the nuclear response.[54,86] They derived the following expression:

$$r_{libr}(t) = \int_0^\infty d\omega\, g(\omega) \exp(-\gamma t/2) \frac{1}{\omega_{eff}} \sin(\omega_{eff} t) \qquad (7)$$

in which $g(\omega)$ is a line shape function, representing the inhomogeneous distribution of librational frequencies, whereas γ is the homogeneous damping rate and $\omega_{eff} = (\omega^2 - \gamma^2/4)^{1/2}$, where ω is the librational frequency. Here, we assume the inhomogeneous distribution to have the form of an antisymmetrized Gaussian of frequency ω_0 and width σ:

$$g(\omega) = \exp\left[\frac{-(\omega - \omega_0)}{2\sigma^2}\right] - \exp\left[\frac{-(\omega + \omega_0)}{2\sigma^2}\right] \qquad (8)$$

which has the property of becoming zero at $\omega = 0$. This model has been used with considerable success to describe the spectral density of neat CS_2 and CS_2 diluted in isopentane. In particular, McMorrow et al. showed that the large shift in the ultrafast spectral density to lower wave number on dilution in isopentane was well described by eq 7, simply by varying the central frequency of the inhomogeneous distribution, ω_0.[32] This is the question we wish to address here: Can the spectral density of the microemulsion also be effectively described by the model of Duppen et al.?

Figure 8a shows a comparison of the $r(t)$ functions from neat CS_2 and the 13/30 microemulsion with those calculated using eq 7. The simulation of the CS_2 data yielded the following parameters: $\omega_0 = 9.0$ ps^{-1}, $\gamma = 1.75$ ps^{-1}, $\sigma = 5.2$ ps^{-1}, and $c = 0.35$. These are in good agreement with the work of both Duppen et al.[54] and McMorrow et al.[32] The parameters required to model the microemulsion data are as follows: $\omega_0 = 6.75$ ps^{-1}, $\gamma = 1.75$ ps^{-1}, $\sigma = 6.0$ ps^{-1}, and $c = 0.15$. As anticipated from the results of McMorrow et al.,[32] a change in the central librational frequency was the dominant factor required to account for the differences between neat CS_2 and the microemulsion. However, a small change in the inhomogeneous line width was also required to simulate the experimental data accurately.

In light of this result, it is interesting to compare the individual effects of changing these two parameters. Parts b and c of Figure 8 show changes in the $r(t)$ functions associated with variation of ω_0 and σ, respectively. The effects of varying either parameter are similar. However, changing the central frequency was found to modify the $r(t)$ function at all times, whereas changes in the width parameter have the greatest effect at early times. Furthermore, σ changes the rising part of the response much more markedly than does variation in ω_0. The result is that the same effect cannot be achieved with both parameters, and variations in both are required to reproduce the experimental observations.

The results of modeling the data support the earlier qualitative conclusions, that the dynamics of CS_2 in a microemulsion are intermediate between those of solvated and neat CS_2, in that a change in central frequency of Im($D(\omega)$) is observed for the microemulsion, but the change is not as great as that observed upon dilution.

Conclusions

The ultrafast dynamics of the oil phase of carbon disulfide−dodecyltrimethylammonium bromide−water (CS_2−DTAB−H_2O) microemulsions have been studied using optically-heterodyne-detected optical Kerr effect (OHD−OKE) spectroscopy. The observed dynamics have been analyzed in the frequency and time domains, using well-established models, and the results have been compared to those for both bulk CS_2 and CS_2 diluted in *n*-alkane solvents.

It is clear from these data that the dynamics of microemulsion-constrained CS_2 differ markedly from those of neat CS_2. Qualitatively, it was found that the librational line shape narrows and shifts to lower frequency in the microemulsion. These effects, however, are not as extensive as those observed for CS_2 diluted in alkanes. However, the results show that a microemulsion-dispersed droplet cannot be thought of as a microscopic pool of bulklike CS_2. Rather, the dynamics are intermediate between bulk and solvated CS_2. These observations have

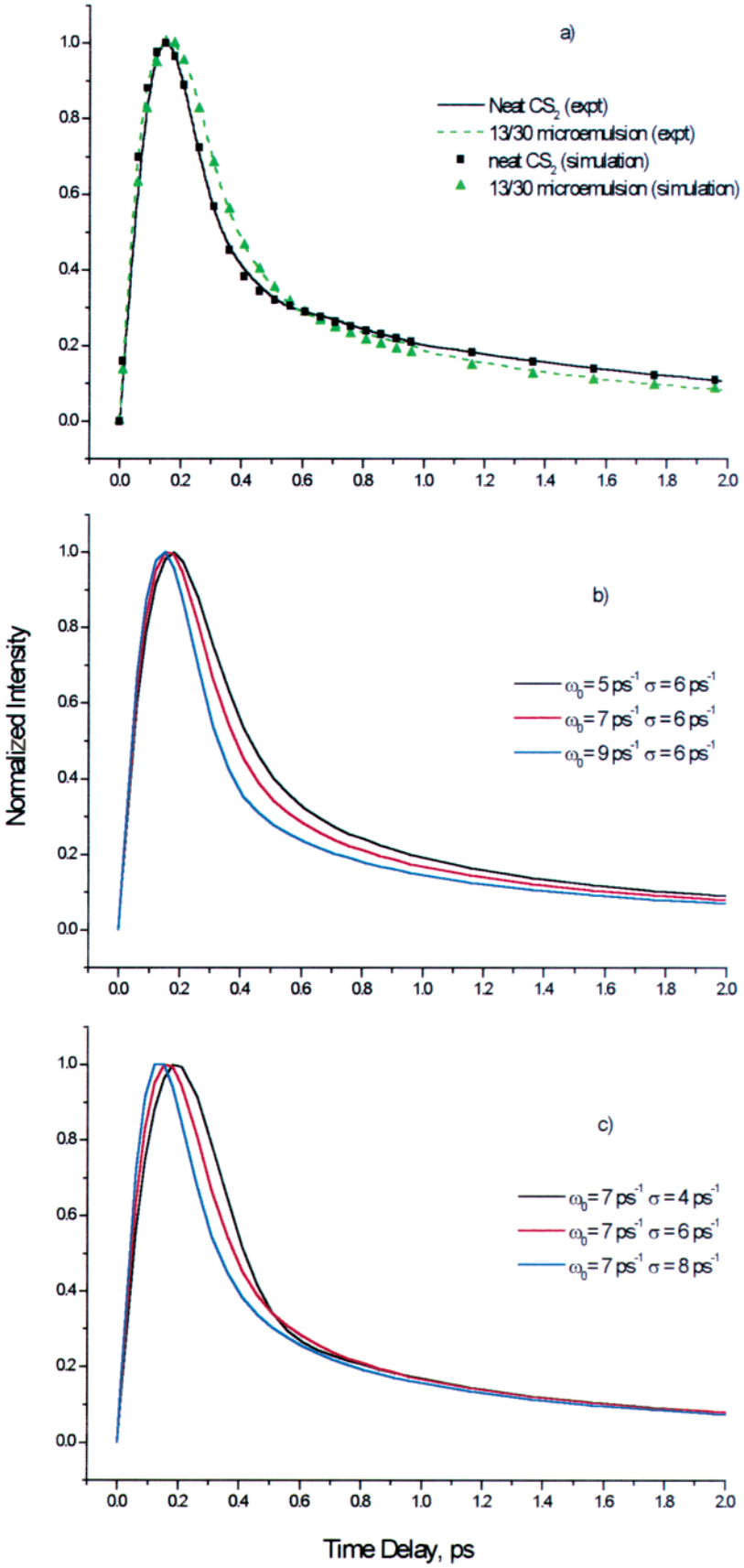

Figure 8. (a) Comparison of simulated (eq 6) and experimental data for neat CS_2 and 13/30 microemulsion. (b) Simulated changes in line shape based upon eq 6 for changing ω_0 with σ fixed. (c) Simulated changes in line shape based upon eq 6 for changing σ with ω_0 fixed.

been borne out by the application of a quantum mechanical harmonic oscillator model, which yields parameters also intermediate between neat and diluted CS_2.

The picosecond-time-scale relaxations, associated with rotational diffusion of the CS_2 molecules, occur on similar time scales in the microemulsions and in neat CS_2 and CS_2 dissolved

in fluid solvents. However, the viscosities of the microemulsions are very large. This result indicates the decoupling between microscopic and macroscopic dynamics in these systems.

The marked nonexponentiality of the picosecond dynamics of the microemulsion shows similarities with the dynamics of CS_2 diluted in long *n*-alkane chains (but not other solvents) and supports the notion[30] of the formation of an inhomogeneous distribution of CS_2 environments in both the alkanes and the microemulsions. The origin and nature of the distribution of environments, however, are unclear.

OHD−OKE studies of microemulsions are currently being extended to other systems, including the exchange of the oil phase for styrene and the study of dispersed-phase dynamics in inverse micelles. In either case, it will be important to characterize the sample morphology further, in an effort to understand the complex rheological behavior already observed for the CS_2−DTAB−H_2O system.

Acknowledgment. The authors would like to thank EPSRC for financial support for this research. A.A.J. is grateful to EPSRC for a studentship.

References and Notes

(1) Birdi, K., Ed. *Handbook of Surface and Colloid Chemistry*; CRC Press: Boca Raton, FL, 1997.
(2) Degiorgio, V. *Fisica Degli Anfifili: Micelle, Vesicole e Microemulsioni*; North-Holland: Amsterdam, 1983.
(3) Bourrel, M.; Schechter, R. S. *Microemulsions and Related Systems*; Surfactant Science Series, Vol. 30; Marcel Dekker: New York, 1988.
(4) Paul, B. K.; Moulik, S. P. *Curr. Sci.* **2001**, *80*, 990.
(5) *Non Equilibrium Behaviour of Colloidal Dispersions*; to be published as Faraday Discussions, No. 123; University of Edinburgh: Edinburgh, U.K., 2002.
(6) Wang, W.; Asher, S. A. *J. Am. Chem. Soc.* **2001**, *123*, 12528.
(7) Lotshaw, W. T.; McMorrow, D.; Thantu, N.; Melinger, J. S.; Kitchenham, R. *J. Raman Spectrosc.* **1995**, *26*, 571.
(8) Kinoshita, S.; Kai, Y.; Ariyoshi, T.; Shimada, Y. *Int. J. Mod. Phys. B* **1996**, *10*, 1229.
(9) Smith, N. A.; Meech, S. R. *Int. Rev. Phys. Chem.* **2002**, *21*, 75.
(10) Castner, E. W., Jr.; Maroncelli, M. *J. Mol. Liq.* **1998**, *77*, 1.
(11) Fleming, G. R.; Cho, M. *Annu. Rev. Phys. Chem.* **1996**, *47*, 109.
(12) Rips, I.; Jortner, J. *J. Chem. Phys.* **1987**, *87*, 2090.
(13) Yoshihara, K. *Adv. Chem. Phys.* **1999**, *107*, 371.
(14) Boyd, J. E.; Briskman, A.; Sayes, C. M.; Mittleman, D.; Colvin, V. *J. Phys. Chem. B* **2002**, *106*, 6346.
(15) Boyd, J. E.; Briskman, A.; Colvin, V. L.; Mittlemanm, D. M. *Phys. Rev. Lett.* **2001**, *87*, 147401.
(16) Venables, D. S.; Huang, K.; Schmuttenmaer, C. A. *J. Phys. Chem. B* **2001**, *105*, 9132.
(17) Willard, D. M.; Riter, R. E.; Levinger, N. E. *J. Am. Chem. Soc.* **1998**, *120*, 4151.
(18) Riter, R. E.; Undiks, E. P.; Levinger, N. E. *J. Am. Chem. Soc.* **1998**, *120*, 6062.
(19) Riter, R. E.; Undiks, E. P.; Kimmel, J. R.; Pant, D. D.; Levinger, N. E. *J. Phys. Chem. B* **1998**, *102*, 7931.
(20) Shirota, H.; Horie, K. *J. Phys. Chem. B* **1999**, *103*, 1437.
(21) Bhattacharyya, K.; Bagchi, B. *J. Phys. Chem. A* **2000**, *104*, 10603.
(22) Lotshaw, W. T.; McMorrow, D.; Kenney-Wallace, G. A. *Proc. SPIE* **1988**, *981*, 20.
(23) McMorrow, D.; Lotshaw, W. T. *J. Phys. Chem.* **1991**, *95*, 10395.
(24) Back, R.; Kenney-Wallace, G. A.; McMorrow, D.; Lotshaw, W. T. *Chem. Phys. Lett.* **1992**, *191*, 423.
(25) McMorrow, D.; Lotshaw, W. T. *Chem. Phys. Lett.* **1993**, *201*, 369.
(26) McMorrow, D.; Lotshaw, W. T. *Chem. Phys. Lett.* **1990**, *174*, 85.
(27) McMorrow, D.; Lotshaw, W. T.; Kenney-Wallace, G. A. *IEEE J. Quantum Electron.* **1988**, *24*, 443.
(28) McMorrow, D.; Lotshaw, W. T. *Chem. Phys. Lett.* **1991**, *178*, 69.
(29) Palese, S.; Mukamel, S.; Miller, R. J. D.; Lotshaw, W. T. *J. Phys. Chem.* **1996**, *100*, 10380.
(30) McMorrow, D.; Thantu, N.; Melinger, J. S.; Kim, S. K.; Lotshaw, W. T. *J. Phys. Chem.* **1996**, *100*, 10389.
(31) Kalpouzos, C.; McMorrow, D.; Lotshaw, W. T.; Kenney-Wallace, G. A. *Chem. Phys. Lett.* **1988**, *150*, 138.
(32) McMorrow, D.; Thantu, N.; Kleiman, V.; Melinger, J. S.; Lotshaw, W. T. *J. Phys. Chem. A* **2001**, *105*, 7960.
(33) Chang, Y. J.; Castner, E. W., Jr. *J. Phys. Chem.* **1994**, *98*, 9712.
(34) Chang, Y. J.; Castner, E. W., Jr. *J. Chem. Phys.* **1993**, *99*, 113.
(35) Chang, Y. J.; Castner, E. W., Jr. *J. Chem. Phys.* **1993**, *99*, 7289.
(36) Chang, Y. J.; Castner, E. W., Jr. *J. Phys. Chem.* **1996**, *100*, 3330.
(37) Wiewior, P. P.; Shirota, H.; Castner, E. W., Jr. *J. Chem. Phys.* **2002**, *116*, 4643.
(38) Smith, N. A.; Lin, S.; Meech, S. R.; Shirota, H.; Yoshihara, K. *J. Phys. Chem. A* **1997**, *101*, 9578.
(39) Smith, N. A.; Lin, S.; Meech, S. R.; Yoshihara, K. *J. Phys. Chem. A* **1997**, *101*, 3641.
(40) Shirota, H.; Yoshihara, K.; Smith, N. A.; Lin, S.; Meech, S. R. *Chem. Phys. Lett.* **1997**, *281*, 27.
(41) Smith, N. A.; Meech, S. R. *Faraday Discuss.* **1997**, *108*, 35.
(42) Smith, N. A.; Meech, S. R. *J. Phys. Chem. A* **2000**, *104*, 4223.
(43) Kamada, K.; Ueda, M.; Sakaguchi, T.; Ohta, K.; Fukumi, T. *Chem. Phys. Lett.* **1996**, *249*, 329.
(44) Kamada, K.; Ueda, M.; Ohta, K.; Wang, Y.; Ushida, K.; Tominaga, Y. *J. Chem. Phys.* **1998**, *109*, 10948.
(45) Quitevis, E. L.; Neelakandan, M. *J. Phys. Chem.* **1996**, *100*, 10005.
(46) Neelakandan, M.; Pant, D.; Quitevis, E. L. *Chem. Phys. Lett.* **1997**, *265*, 283.
(47) Neelakandan, M.; Pant, D.; Quitevis, E. L. *J. Phys. Chem. A* **1997**, *101*, 2936.
(48) Cong, P.; Deuel, H. P.; Simon, J. D. *Chem. Phys. Lett.* **1995**, *240*, 72.
(49) Cong, P.; Simon, J. D.; She, C. Y. *J. Chem. Phys.* **1996**, *104*, 962.
(50) Wynne, K.; Galli, C.; Hochstrasser, R. M. *Chem. Phys. Lett.* **1992**, *193*, 17.
(51) Kinoshita, S.; Kai, Y.; Yamaguchi, M.; Yagi, T. *Phys. Rev. Lett.* **1995**, *75*, 148.
(52) Kinoshita, S.; Kai, Y.; Yamaguchi, M.; Yagi, T. *Chem. Phys. Lett.* **1995**, *236*, 259.
(53) Kinoshita, S.; Kai, Y.; Watanabe, Y. *Chem. Phys. Lett.* **1999**, *301*, 183.
(54) Steffen, T.; Meinders, N. A. C. M.; Duppen, K. *J. Phys. Chem. A* **1998**, *102*, 4213.
(55) Jansen, T. I. C.; Pugzlys, A.; Crîngus, G. D.; Snijders, J. G.; Duppen, K. *J. Chem. Phys.* **2002**, *116*, 9383.
(56) Bartolini, P.; Ricci, M.; Torre, R.; Righini, R.; Sánta, I. *J. Chem. Phys.* **1999**, *110*, 8653.
(57) Ricci, M.; Bartolini, P.; Chelli, R.; Cardini, G.; Califano, S.; Righini, R. *Phys. Chem. Chem. Phys.* **2001**, *3*, 2795.
(58) Idrissi, A.; Bartolini, P.; Ricci, M.; Righini, R. *J. Chem. Phys.* **2001**, *114*, 6774.
(59) Idrissi, A.; Ricci, M.; Bartolini, P.; Righini, R. *J. Chem. Phys.* **1999**, *111*, 4148.
(60) Farrer, R. A.; Loughnane, B. J.; Deschenes, L. A.; Fourkas, J. T. *J. Chem. Phys.* **1997**, *106*, 6901.
(61) Loughnane, B. J.; Scodinu, A.; Farrer, R. A.; Fourkas, J. T. *J. Chem. Phys.* **1999**, *111*, 2686.
(62) Shirota, H.; Castner, E. W., Jr. *J. Am. Chem. Soc.* **2001**, *123*, 12877.
(63) Stankus, J. J.; Torre, R.; Fayer, M. D. *J. Phys. Chem.* **1993**, *97*, 9478.
(64) Loughnane, B. J.; Farrer, R. A.; Scodinu, A.; Reilly, T.; Fourkas, J. T. *J. Phys. Chem. B* **2000**, *104*, 5421.
(65) Loughnane, B. J.; Farrer, R. A.; Scodinu, A.; Fourkas, J. T. *J. Chem. Phys.* **1999**, *111*, 5116.
(66) Loughnane, B. J.; Scodinu, A.; Fourkas, J. T. *J. Phys. Chem. B* **1999**, *103*, 6061.
(67) Loughnane, B. J.; Farrer, R. A.; Fourkas, J. T. *J. Phys. Chem. B* **1998**, *102*, 5409.
(68) Farrer, R. A.; Loughnane, B. J.; Fourkas, J. T. *J. Phys. Chem. A* **1997**, *101*, 4005.
(69) Gan, L. M.; Lian, N.; Chew, C. H.; Li, G. Z. *Langmuir* **1994**, *10*, 2197.
(70) Puig, J. E.; Pérez-Gonzáles, M.; Macías, E. R.; Rodriguez, B. E.; Kaler, E. W. *Colloid Polym. Sci.* **1993**, *271*, 114.
(71) Maroncelli, M. *J. Chem. Phys.* **1991**, *94*, 2084.
(72) Ladanyi, B. M. In *Electron Transfer in Condensed Media*; Kornyshev, A. A., Tosi, M., Ulstrup, J., Eds.; World Scientific: Singapore, 1997; pp 110−129.
(73) Ladanyi, B. M.; Stratt, R. M. *J. Phys. Chem.* **1996**, *100*, 1266.
(74) Saito, S.; Ohmine, I. *Phys. Rev. Lett.* **2002**, *88*, 207401.
(75) Jansen, T. I. C.; Snijders, J. G.; Duppen, K. *J. Chem. Phys.* **2001**, *114*, 10910.
(76) Ji, X.; Ahlborn, H.; Space, B.; Moore, P. B. *J. Chem. Phys.* **2000**, *113*, 8693.
(77) Stassen, H.; Steele, W. A. *J. Chem. Phys.* **1999**, *110*, 7382.
(78) Fleming, W. R. *J. Agric. Res. (Washington, DC)* **1926**, *33*, 17.
(79) Heimenz, P. C. *Principles of Colloid and Surface Chemistry*; Marcel-Dekker: New York, 1986.
(80) Bergstrom, M.; Pedersen, J. S. *Phys. Chem. Chem. Phys.* **1999**, *1*, 4437.
(81) Malliaris, A.; Lang, J.; Zana, R. *J. Colloid Interface Sci.* **1986**,

110, 237.
(82) Bergenholtz, J.; Romagnoli, A. A.; Wagner, N. J. *Langmuir* **1995**, *11*, 1559.
(83) Phillips, J. N. *Trans. Faraday. Soc*. **1955**, *51*, 561.
(84) Kivelson, D.; Madden, P. A. *Annu. Rev. Phys. Chem*. **1980**, *31*, 523.
(85) Berne, B. J.; Pecora, R. *Dynamic Light Scattering*; Wiley: New York, 1976.
(86) Steffen, T.; Fourkas, J. T.; Duppen, K. *J. Chem. Phys.* **1996**, *105*, 7382.
(87) Lide, D. R., Ed. *CRC Handbook of Chemistry and Physics*, 81st ed.; CRC Press: Boca Raton, FL, 2000−2001.